The critical points of strongly coupled lattice QCD at nonzero chemical potential

Ian M. Barbour* and Susan E. Morrison*
Department of Physics and Astronomy, University of Glasgow, Glasgow G12 8QQ, Scotland

Elyakum G. Klepfish*
Department of Physics, King's College London, London WC2R 2LS, United Kingdom

John B. Kogut
University of Illinois at Urbana–Champaign, 1110 West Green Street, Urbana, Illinois 61801-3080

Maria-Paola Lombardo
Zentrum für interdisziplinäre Forschung, Universität Bielefeld, D-33615 Bielefeld, Germany
(Received 30 May 1997)

We study QCD at nonzero quark density, zero temperature, infinite coupling using the Glasgow algorithm. An improved complex zero analysis gives a critical point μ_c in agreement with that of chiral symmetry restoration computed with strong coupling expansions, and monomer-dimer simulations. We observe, however, two unphysical critical points: the onset for the number density μ_0, and μ_s the saturation threshold, coincident with pathological onsets observed in past quenched QCD calculations. An analysis of the probability distributions for particle number supports our physical interpretation of the critical point μ_c, and offers a new intepretation of μ_0, which confirms its unphysical nature. The perspectives for future lattice QCD calculations of the properties of dense baryonic matter are briefly discussed. [S0556-2821(97)02121-8]

PACS number(s): 12.38.Mh, 11.15.Ha, 12.38.Gc

I. INTRODUCTION

Numerical simulations of lattice QCD at high temperatures are making quantitative theoretical predictions which will be confronted with experiments at the BNL Relativistic Heavy Ion Collider (RHIC) and the CERN Large Hadron Collider (LHC) [1]. However, numerical simulations of QCD in an environment rich in baryons lags far behind. Phenomenologically we know that nuclear matter can exist up to a density of four times ordinary matter in neutron stars, and that higher density will eventually induce deconfinement and chiral symmetry restoration because of asymptoptic freedom. Current estimates from phenomenological nuclear models [2] place the critical chemical potential between 1000 and 1600 MeV, and the critical baryon density between 2 or 20 times that of ordinary nuclear matter.

As it is well known, the reason behind this poor knowledge is the lack of a reliable calculational scheme for lattice QCD at high baryon densities [3]. A solid theoretical formulation for finite density QCD was made ten years ago [4,5], but, since the resulting action is complex, probabilistic simulation methods fail. Early approaches considered the quenched approximation, which omits the complex fermion determinant, but it produced unphysical results [6–10]. To obtain reliable results the determinant should be included, and the Glasgow method has been proposed to tackle this challenge [11–17]. Although we are ultimately interested in the weak coupling, continuum limit, the strong coupling limit of QCD is attractive for several reasons: (1) There are analytic results coming from the strong coupling expansion [18–20] and numerical results from monomer-dimer simulations [21]; (2) the theory confines and spontaneously breaks chiral symmetry. In this paper we will use these features of strongly coupled lattice QCD to test and shed light on simulation methods which could be used at any coupling [22].

This paper is organized into two main sections, Method and Results.

Method is part review and part illustration of our method of analysis. We first review the Glasgow method, and the relevant observables (Sec. II A). We continue by illustrating some features which will help our numerical analysis. We will first discuss (Sec. II B) the pathologies found in calculations on isolated configurations. In Sec. II C we will discuss how the Glasgow algorithm can escape from these single-configuration pathologies, and build the physical signatures for the critical point μ_c where chiral symmetry is restored.

In *Results*, after discussing some generalities of the generation of the gauge ensemble (Sec. III A), we show that the Glasgow method results for the baryon current inherit some of the quenched or single-configuration pathologies (Sec. III B). Nevertheless, we will successfully measure the critical chemical potential μ_c (Sec. III C) and we will discuss in detail the interplay of successes and failures of the results. Comprehensive results for an extended range of masses are given in Sec. III D. In Sec. III E we will present an alternative reanalysis of the critical region which will use probability distributions. We will confirm there the estimate of the critical point μ_c, and we will offer a new intepretation of the pathological region.

We conclude with a brief summary and discussion.

*Affiliated with the UKQCD Collaboration.

 © 1997 The American Physical Society

II. METHOD

Given the failure of the quenched approximation to deal with the problem of the chiral phase transition at high quark density, the natural conclusion is that dynamical quark simulations are essential. However, the complex measure of the functional integration with nonzero chemical potential poses a severe problem for such simulations. One simulation method which circumvents this problem is based on the expansion of the grand-canonical partition function (GCPF) in powers of the fugacity. The GCPF (Z) can be written as the ensemble average $\langle |M(\mu,m)|/|M(0,m)| \rangle$ where $|M(\mu,m)|$ is the fermion determinant at chemical potential μ and quark mass m in lattice units (lattice spacing $a=1$): i.e.,

$$Z=\frac{\int [dU][dU^{\dagger}]|M(\mu,m)|e^{-S_g[U,U^{\dagger}]}}{\int [dU][dU^{\dagger}]|M(0,m)|e^{-S_g[U,U^{\dagger}]}}, \tag{1}$$

where U are matrices representing the gauge degrees of freedom and S_g is the standard Wilson gauge action. The fermion matrix M is that describing four flavors of staggered fermions.

The fermionic determinant can be expressed explicitly as a function of μ by

$$\det[M(\mu,m)]=e^{-3\mu n_s^3 n_t}\det(P-e^{\mu}). \tag{2}$$

The lattice size is $n_s^3 n_t$ and P is the propagator matrix (independent of μ) [7]

$$P=\begin{pmatrix} -GV & V \\ -V & 0 \end{pmatrix}, \tag{3}$$

where G contains all the spacelike gauge links and the quark bare mass, and V all the forward timelike links of the fermionic matrix M.

$\det[M(\mu,m)]$ can be computed in a basis where the propagator matrix is diagonal:

$$\det[M(\mu,m)]=e^{-3\mu n_s^3 n_t}\prod_{k=1}^{6n_s^3 n_t}(\lambda_k-e^{\mu}). \tag{4}$$

We recognize that the zeros of the determinant in the e^{μ} plane are the eigenvalues of the propagator matrix. The symmetry of the eigenvalues of the propagator matrix $\lambda_{k+j}=e^{i2\pi j/n_t}\lambda_k$ for $j=0$ to n_t-1, together with the polynomial decomposition

$$\prod_{j=0}^{n_t-1}(e^{i2\pi j/n_t}\beta-x)=(\beta^{n_t}-x^{n_t}) \tag{5}$$

yield the equivalent representation

$$\det[M(\mu,m)]=e^{-3\mu n_s^3 n_t}\prod_{k=1}^{6n_s^3}(\lambda_k^{n_t}-e^{\mu n_t}) \tag{6}$$

and dictates the general structure of the characteristic polynomial $\det[M(\mu,m)]$

$$\det[M(\mu,m)]=\sum_{k=-3n_s^3}^{3n_s^3} b_i e^{k\mu n_t}. \tag{7}$$

Note the dependence on μ is now via the fugacity $f=e^{\mu n_t}$.

Hence, measurement of the average of the characteristic polynomials [normalized by $|M(0,m)|$] in the ensemble generated at update mass m and $\mu=0$ will give $Z(\mu,m)$ explicitly as a function of μ at that mass.

This representation leads to a polynomial expansion of $Z(\mu)$ in powers of the fugacity whose coefficients are functions of the gluonic fields.

$$Z(\mu)=\sum_{k=-3n_s^3}^{3n_s^3}\langle b_i\rangle e^{k\mu T}=\sum_{k=-3n_s^3}^{3n_s^3} Q_k f^k. \tag{8}$$

This expansion is just that of the GCPF expanded in terms of the canonical partition functions (CPF's) for a fixed number of quarks (antiquarks) on the lattice. Thermodynamical averages, which can be calculated as logarithmic derivatives of the GCPF, are then given explicitly as functions of μ.

The relative value of the CPF's can characterize the properties of the system as well. For example, the relative weight of the triality-bearing to the triality-zero CPF's can signal whether the system is in the confined or deconfined phase. In the confined phase the ensemble average of the triality-bearing CPF's must be zero. This leads to

$$Z(\mu)=\sum_{k=n_s^3}^{n_s^3} Q_{3k} f^{3k}. \tag{9}$$

One can also explore the phase structure of the simulated system by examining the distribution of the zeros of the GCPF in the complex chemical potential (or fugacity) plane [23,24]. These zeros correspond to the singularities of the thermodynamic potential and will converge in the thermodynamic limit, ($L\to\infty$) towards any critical μ in the physical domain.

In the following we also show that one can regard the zeros of the averaged characteristic polynomial as the ''proper'' ensemble average of the eigenvalues of the propagator matrix. This interpretation of the zeros as reflecting the ensemble average of the eigenvalues could be important in the interpretation of ''unexpected'' onset chemical potentials in ensembles of limited statistics.

A. Observables

The starting point of our analysis is the GCPF Z computed with the Glasgow algorithm. Our raw data are the CPF's Q_N and our basic observables are the particle number density and the zeros of the GCPF in the complex fugacity plane.

Most of our discussions will consider the current $\langle J_0(\mu,m)\rangle$ or equivalently the particle number density, defined as

$$\langle J_0(\mu,m)\rangle = \frac{1}{V}\frac{\partial \ln[Z(\mu,m)]}{\partial\mu} = \frac{1}{V}\frac{\partial \ln\langle \det[M(\mu,m)]\rangle}{\partial\mu}. \tag{10}$$

The singular behavior of the current can result from singularities in the density of baryonic states (particularly apparent in the zero-temperature limit). These singularities could be purely lattice artifacts and vanish in the continuum limit. However, they may instead reflect continuum spectral features, such as gaps in the spectrum or abrupt changes in the dispersion relation of the baryonic excitations. A chiral phase transition is one such possibility. A spectrum of chirally symmetric baryonic excitations will follow a gapless relativistic dispersion relation, contrary to the dispersion of particles with broken chiral symmetry. If the disappearance of the mass gap occurs together with the deconfinement transition, quark states will emerge instead of collective colorless baryonic excitations. Thus, the μ dependence of J_0 should determine the phase structure of dense baryonic matter, an alternative to the evaluation of the chiral condensate.

Differentiating the action with respect to μ reveals the operator form of the charge, and one sees that the current is the expectation value of the number of paths through the links in the time direction [4]. In this sense the current can be defined on isolated configurations, where it reduces to

$$J_0^i(\mu,m) = \frac{1}{V}\frac{\partial \ln\{\det[M(\mu,m)]\}}{\partial\mu}. \tag{11}$$

In the quenched ensemble $\ln[\det(M)]$ is differentiated *before* taking the statistical average,

$$\langle J_0\rangle^q(\mu,m) = \frac{1}{V}\left\langle \frac{\partial \ln\{\det[M(\mu,m)]\}}{\partial\mu}\right\rangle, \tag{12}$$

and we recognize that

$$\langle J_0(\mu,m)\rangle^q = \langle J_0^i(\mu,m)\rangle. \tag{13}$$

In the following the μ and m dependence will be left implicit wherever this does not create ambiguities.

B. Failures on isolated configurations and the quenched model

The early work by Gibbs [7] made it clear that the behavior of some observables measured on isolated configurations at finite density can be pathological. Since the analysis of isolated configurations is a necessary step in any lattice simulation, the impact of his result may be broader than its original motivation— to understand the pathologies of the quenched approximation.

Our renewed interest was prompted by two considerations. First, our results presented in Sec. III A below show clear relics of the quenched pathologies discussed in Gibbs' paper: the onset μ_0 where the current J_0 departs from zero is at half the pion mass. Second, published results on four fermion models [25,26] do not have such pathologies. However, both models share the same pattern of chiral symmetry breaking, and both models have Goldstone modes. Why, then, is there a difference at finite density? We decided to reexamine the behavior of observables on isolated configurations in order to test the Gibbs scenario in a more general framework, and to gain some understanding of the process of statistical averaging in the two models. This paper is devoted to QCD, and the results for four fermion models will be presented elsewhere.

First consider the behavior of the current on isolated configurations. J_0^i follows from Eqs. (11) and (4):

$$J_0^i = -1 + \frac{1}{V}\sum_{i=1}^{6V} z/(z-\lambda_i) \tag{14}$$

(here and in the following we use Gibbs' notation $z=e^{\mu}$ [7]). In the zero-temperature case the sum over complex poles can be conveniently done by contour integration, yielding

$$J_0^i = \frac{1}{V}\sum_{1<|\lambda_i|<e^{\mu}} 1. \tag{15}$$

The threshold for the current J_0 on isolated configurations is triggered by the lowest zero of the determinant. In turn, the zeros of the determinant are given by the eigenvalues of the propagator matrix that, as emphasized by Gibbs, are controlled by the mass spectrum of the theory. The argument, which we briefly summarize for the sake of completeness, requires the calculation of the hadronic spectrum on replicated lattices, i.e., lattices which have been strung together d times in the time direction and the limit $d\to\infty$ is taken, in order to replace finite sums with contour integrations. This procedure is justifiable at zero temperature.

The expression for the inverse of the fermion matrix, $G(t_1,t_2)$, on the replicated lattices reads (slightly simplifying Gibbs' notation)

$$G(t_1,t_2) = \sum_k A_a \lambda_k^{t_1-t_2}, \tag{16}$$

where the A_a are the amplitudes which can be related to the eigenvectors of the propagator matrix, and the λ_k are the corresponding eigenvalues.

Equation (16) shows that the exponential decay of $G(t_1,t_2)$ at large timelike separation is controlled by the eigenvalues of the propagator matrix. In other words, the eigenvalue spectrum calculated on isolated configurations should be closely related to the physical mass spectrum. In particular, Gibbs concluded that the smallest mass state m_π is related to the lowest eigenvalue:

$$m_\pi = 2\ln|\lambda_{\min}|. \tag{17}$$

This identification was clear in simulations done by Gibbs because the pion propagator was very similar configuration by configuration although, strictly speaking, masses are properties only of the statistical ensemble.

The Gibbs argument has been reformulated and verified by Davies and Klepfish [8]. Pathologies of isolated configurations, the role of confinement, and other issues are also

discussed in [9,10]. All of these works confirm that on isolated configurations there is a singularity at a value of the chemical potential close to half the pion mass.

Therefore, the results on isolated configurations are qualitatively different from those expected of the statistical ensemble.

Some of the problems with the quenched model can be understood from Eq. (13): the quenched current is a simple average of the one-configuration current, and the quenched ensemble retains the pathological features observed on isolated configurations.

C. The statistical ensemble and the full model

We can now focus on the interplay between the one-configuration or quenched results and ensemble results. How can statistical averaging remove the problems observed on isolated configurations? Equivalently, how can the Glasgow averaging discussed above improve upon the quenched approximation?

Consider the fugacity expansion for Z, Eq. (8). By reinstating a factor $e^{3n_s^3 n_t \mu}$ we see that Z is a polynomial of degree $6n_s^3 n_t = 6V$ in the variable $z = e^{\mu}$. Z can then be written in terms of its zeros α_i in the z plane:

$$Z = e^{3V\mu} \prod_{i=1}^{6V} (z - \alpha_i). \tag{18}$$

Recall that $Z = \langle \det(M) \rangle$ and compare formulas (18) and (4) which we rewrite here:

$$\det M = e^{3V\mu} \prod_{i=1}^{6V} (z - \lambda_i). \tag{19}$$

We see that the zeros of the partition function are the ''proper'' ensemble average of the eigenvalues of the fermionic propagator matrix, or, equivalently, of the zeros of the determinant.

Manipulations analogous to those of Eqs. (14) and (15) lead to the current

$$J_0 = \frac{1}{V} \sum_{1 < |\alpha_i| < e^{\mu}} 1. \tag{20}$$

Let us search for other critical points past the first onset. From Eq. (20) we see that discontinuities in J_0 are associated with a high density of zeros on circles with radius e^{μ_c} in the fugacity plane. More generally, the density of the modulos of zeros in the e^{μ} plane is the derivative of J_0 with respect to μ, i.e., the quark number susceptibility. Interestingly, the relevant quantities controlling the critical behavior of the current are indeed the modulos of the complex zeros.

It is worth noticing that, once the $Z3$ symmetry is enforced [Eq. (9)],

$$Z = e^{3n_s^3 \mu} \prod_{i=1}^{2V} (z^3 - \beta_i). \tag{21}$$

The zeros in the complex plane z should then come in triplets, corresponding to cubic roots of certain complex numbers β_i. *In principle* (in practice things can be very different) the effect of the $Z3$ symmetry can simply amount to a redistribution of phases with no effect on the moduli. That would not affect the critical behavior, since the critical behavior is triggered by the moduli themselves. The unphysical quenched onsets could certainly survive the $Z3$ symmetry of the full ensemble.

The zeros of the partition function drive the critical behavior of the full model as the zeros of the determinant drive the critical behavior of isolated configurations, hence of the quenched model. In the process of going from the zeros of the determinant to the zeros of the grand canonical partition function, the pathological results observed on isolated configurations should turn into the physics of the full model: the fake critical points should disappear, the real phase transitions of the full model should emerge.

III. RESULTS

We present here our numerical results. All the background material, when not explicitly referenced, can be found in the previous section.

The generation of the configurations of gauge fields is described in *the ensemble*. In *the number density* we review past results from the quenched approximation, from the monomer-dimer simulation of the full four-flavor model and from the strong coupling expansion of the four-flavor model. We present the results obtained with the Glasgow method on various lattice sizes, and we highlight the main similarities and differences among the Glasgow results and the above-mentioned ones. A discussion of finite size effects is presented as well. In this and in the subsequent subsection, the emphasis is on the presentation of the main features of the results. We then limit ourselves to a discussion of one representative mass value, $m_q = 0.1$.

In *the determination of the critical point* we focus on the analysis of the complex zeros in the e^{μ} plane. We contrast the pattern of zeros with that of the eigenvalues of the fermion propagator. We show how simulations of the full model produce a clear signature for the critical point μ_c.

In *light and heavy masses* we will present our complete set of results. The light masses will offer information about the chiral limit. We confirm that our estimate μ_c remains constant, and different from zero when $m \to 0$. We demonstrate the dependence of μ_c on the bare mass in the heavy quark regime. In the summary plot the results are compared with the strong coupling expansion, and the monomer-dimer calculations.

The analysis of the probability distribution consists of a self-consistent analysis of the critical region which exploits the form of the probability distribution as a function of the chemical potential. This analysis further validates our estimate of the critical point μ_c and, in addition, offers a new intepretation of the onset region μ_o.

A. The ensemble

The Glasgow algorithm takes as input an ensemble of configurations at zero chemical potential. At infinite gauge coupling we can generate configurations either with the usual hybrid Monte Carlo procedure or just choosing random SU(3) matrices — this corresponds to a different normaliza-

tion for the partition function. First, we reproduced the results of Barbour, Davies, and Sabeur [11], which show that the reweighting actually works on a 2^4 lattice provided the statistics are high enough. Some preliminary runs were performed on a 4^4 lattice to check that the results were indeed independent of the algorithm chosen for the generation of the configuration. We finally selected a random generator which produces decorrelated configurations.

We will present results on a 6^4 lattice for bare mass values ranging from 0.05 to 1.5 and on a 8^4 lattice for masses 0.08 and 0.1. The number of gauge field configurations analyzed ranges from a small sample of 25 on the 8^4 lattice $m_q=0.08$, $\simeq$100 configurations on the same lattice, $m_q=0.1$, and several hundred configurations on the 6^4 lattices.

B. The number density

We studied $m_q=0.1$ on 6^4 lattices where we can contrast the results with those obtained (1) in the quenched case, (2) with the monomer-dimer simulation, and (3) with the analytic results of the strong coupling expansions. Let us briefly review methods (2) and (3).

The monomer-dimer approach (valid only at infinite coupling) writes the strong coupling action in a fashion suitable for computer simulations. It begins with the standard lattice QCD action with four flavors of staggered fermions and integrates out the completely disordered gauge fields. Confinement is enforced exactly and the short-ranged interactions between fermions allow the Grassman integrals to also be done exactly. The resulting action can be interpreted graphically in terms of ''monomers'' and ''dimers,'' familiar constructions in statistical physics. This representation of the theory is well suited for computer simulations since the dreaded sign problem of the fermion determinant is not numerically significant in this basis (on small lattices). Computer simulations at $m_q=0.1$ [21] show a sharp transition at $\mu=0.69(1)$ where the chiral condensate falls from its zero-μ value (essentially) to zero, and the number density J_0 jumps from zero (essentially) to a fully occupied lattice, $J_0=1.0$. These results agree with those of the traditional strong coupling expansion, as they should.

The strong coupling expansion [18–20] at $m_q=0.1$ predicts, in fact, a strong first-order transition at $\mu=0.65$ (the small difference in μ_c can probably be accounted for by $1/d$ corrections). The analytic expressions of the strong coupling expansion show a feature not seen in the monomer-dimer simulations: a mixed phase for $\mu_0<\mu<\mu_s$ where ordinary confined hadronic matter coexists with the saturated lattice phase [10].

The quenched results [10] were characterized by a ''forbidden region'' ranging from $\mu_0=m_\pi/2=0.32$ to $\mu_s\simeq m_B/3\simeq 1.0$. μ_0 and μ_s are close to the extrema of the mixed phase predicted by the strong coupling expansions mentioned above. There is no remnant of the critical point for chiral symmetry restoration $\mu_c\simeq 0.65$ predicted by the same expansion.

Our motivation in undertaking the 6^4 calculations, was, of course, to see results completely different from the quenched calculations and very similar to the monomer-dimer results.

These expectations were only partially borne out. We indeed found a signature at μ_c, but *also* the persistence of μ_0 and μ_s. These results are shown in Fig. 1 for the number density obtained with the Glasgow method on a 6^4 lattice at $m_q=0.1$. The Glasgow results are distinguished from the quenched ones by a small jump at $\mu\simeq 0.7\simeq\mu_c$, suggesting restoration of chiral symmetry. Other than that, the Glasgow and quenched results are very similar.

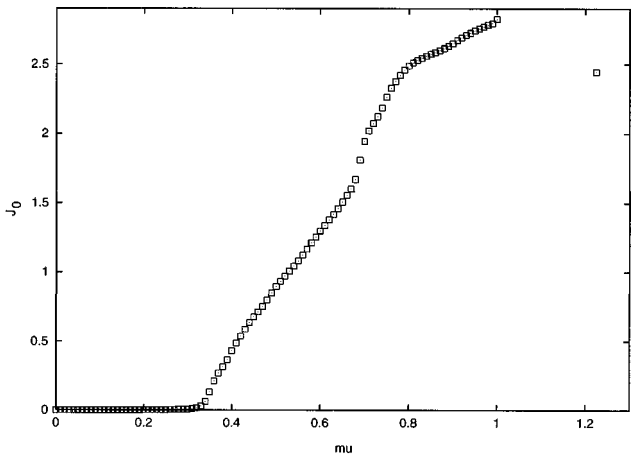

FIG. 1. Quark number density from the Glasgow algorithm. $m_q=0.1$ on a 6^4 lattice. The onset μ_0, and the saturation point μ_s, are the same as the ones observed in the quenched approximation. The critical point for chiral symmetry restoration measured in a monomer-dimer calculation is $\mu_c=0.69(1)$, coincident with the little gap observed in our results. The same monomer-dimer results would, however, predict a very sharp transition with a critical density close to zero, in agreement with the results of the strong coupling expansion.

We then moved to a larger lattice to study the sensitivity to size and temperature. Would the small hint of a discontinuity at $\mu\simeq 0.7$ become more pronounced? Would the dynamical results differ more substantially from the quenched ones?

The answer was in the negative. Neverthless, we did learn something from these runs.

In Fig. 2, we show a detailed comparison of the results on the two lattices, 6^4 and 8^4, $m_q=0.1$ (note the different scales

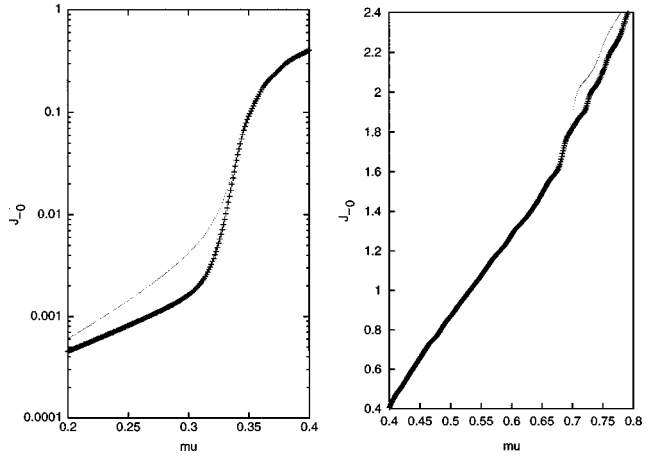

FIG. 2. Finite size effects at $m_q=0.1$. We show details of the critical regions around μ_0 and μ_c for $m_q=0.1$ for two different lattices. The thick lines are for the 8^4 lattice, the thin lines for the 6^4.

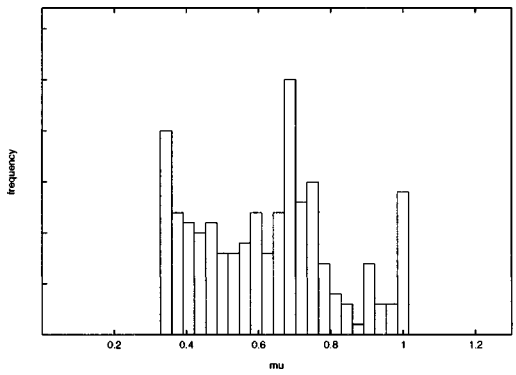

FIG. 3. Histogram of zeros accompanying Fig. 1. Note (a) the peak at $\mu_c = 0.687(15)$ matching the small jump, to be contrasted with the monomer-dimer results $\mu_c = 0.69(1)$, (b) the correspondence of the extrema of the histogram with the onset μ_0 of the current and its saturation μ_s.

on the right and left sides). By blowing up the picture of the number density, we see that the density itself deviates from zero at $\mu \simeq 0$. This effect is very small (note the scale) and it is sensitive to temperature, the number density being suppressed, as expected, on the colder lattice.

The most interesting point is that temperature effects are greatly lessened for $\mu > \mu_0$. One might have well thought that the increase at μ_0 reflects a thermal excitation of baryons. This does not seem to be the case: only for $\mu < \mu_0$ do we observe the expected, physical pattern of finite temperature effects. This disappears for $\mu > \mu_0$. This result supports the belief that the rise at μ_0 is unphysical, as in the quenched approximation. Of course we cannot rule out the possibility that the situation changes on larger lattices, and we refer to [9,10] for discussions on this point.

Temperature effects become apparent again at μ_c, suggesting that μ_c is a threshold of a new phase.

C. The determination of the critical point

We can substanstiate this intepretation of μ_c by examining the zeros of the grand partition function in the complex plane e^{μ}.

The numerical strategy suggested by Sec. II, Eq. (20) is straightforward: observe the distribution of the modulos of the zeros, or, equivalently, search for a strip of high densities in the e^{μ} plane. This criterion is numerically more convenient than the conventional Lee-Yang analysis, which only uses the zero whose imaginary part is closest to the real axes. It is also very natural: it says that the number density counts the density of states in the fermionic sector.

This strategy is demonstrated in Fig. 3 where we show the distribution of zeros (in practice, of the logarithms of their moduli) accompanying Fig. 1. The signal at $\mu_c = 0.687(15)$ is very clear, and in excellent agreement with the monomer-dimer results $\mu_c = 0.69(1)$.

Figure 4 contrasts zeros of the determinant and zeros of the GCPF on an 8^4 lattice. The signal at μ_c in the full model is quite clear.

As discussed above, the upper and lower parts of the figure can also be seen as full and quenched results. As a by-product of our investigation, we see clearly why the search

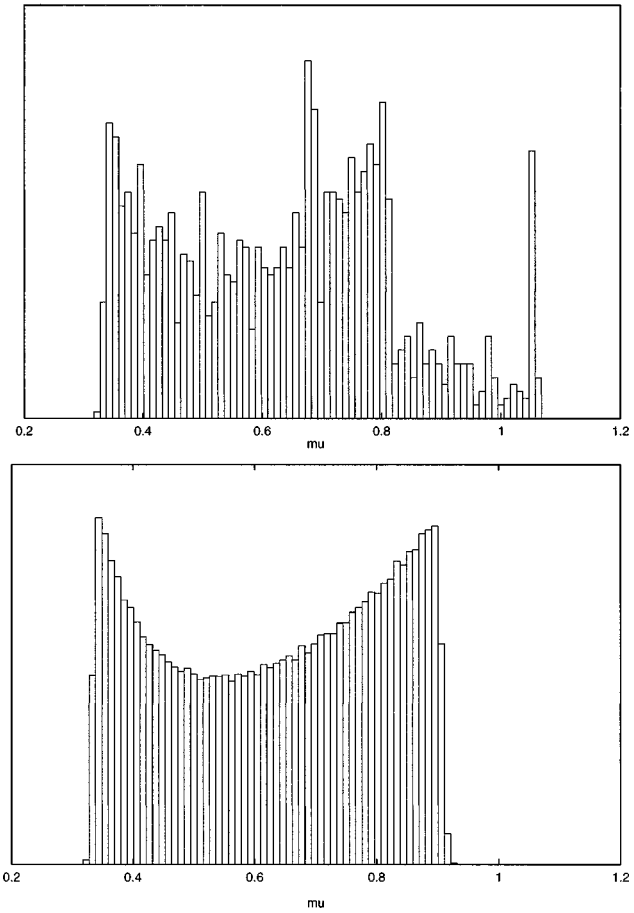

FIG. 4. Histogram of the zeros of the full model (top), and histogram of the zeros of the determinant (bottom), hence of the quenched approximation. $m_q = 0.1$, on an 8^4 lattice.

of further critical points in the quenched calculations was futile [27,10]: the eigenvalue distribution is almost ''flat.''

Unfortunately, the upper and lower parts of the figure also show strong signals at μ_0 and μ_s: the behavior at the two side peaks does not change as we pass from the quenched to the full model. This gives us another view of the puzzling persistence of the onset noticed in the previous subsection. The Glasgow simulation method has failed to reproduce the published monomer-dimer results.

We can also look at the zeros themselves, which we display in Fig. 5. As anticipated in the discussion, we observe a dense line, which follows the prediction $|e^{\mu}| = e^{\mu_c}$. We also see a ring of zeros at half the pion mass, and note that the zeros fill up the entire region $\mu_0 - \mu_s$.

In summary, we have seen how the small discontinuity observed in the current manifests itself in the histogram of zeros: the density of zeros is the *derivative* of the number density, so a small ''discontinuity'' in J_0 corresponds to a distinct signal in the histogram of zeros.

Will more statistics eventually cancel the onsets at μ_0 and μ_s? Even if we have not observed any dramatic effect by increasing the number of configurations, insufficient statistics remains a possibility, especially since Z_3 invariance has not been completely achieved yet, and since it is possible that the precision required to achieve the cancellation of the unwanted onset is prohibitively high. It is also possible that

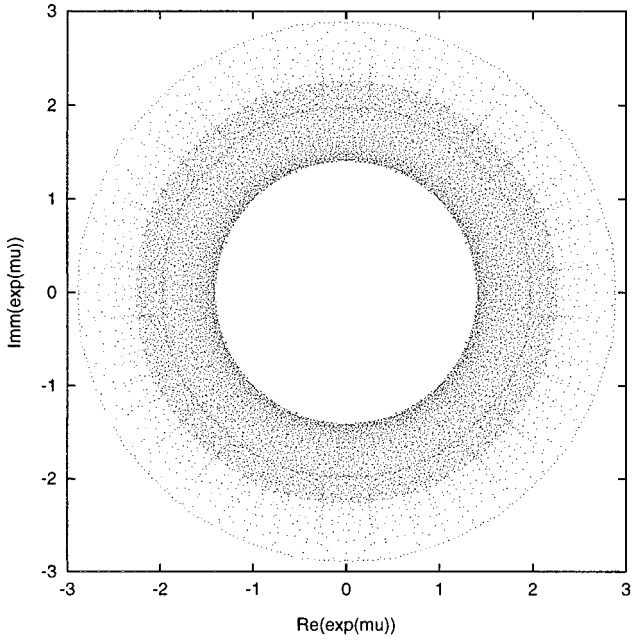

FIG. 5. Zeros in the e^{μ} plane for $m=0.1$ 8^4 lattice. The critical line is the thin line inside the denser region $e^{\mu}=e^{\mu_c}$.

the polynomial representation for the GCPF is ill-conditioned [28].

D. Heavy and light masses

All the results we have discussed above were for $m_q=0.1$. It is instructive to explore both light and heavy masses. Light masses are important for the chiral limit. There we expect the critical point μ_c to remain constant and different from zero. Heavy masses change the critical point and allow a more detailed comparison of our results with the monomer-dimer–strong-coupling approaches.

We studied the sensitivity to the quark mass close to the chiral limit ($0.05<m_q<0.1$). We noted the stability of the central peak and the shift of the lower peak, which is associated with the onset of the current at one-half of the pion mass.

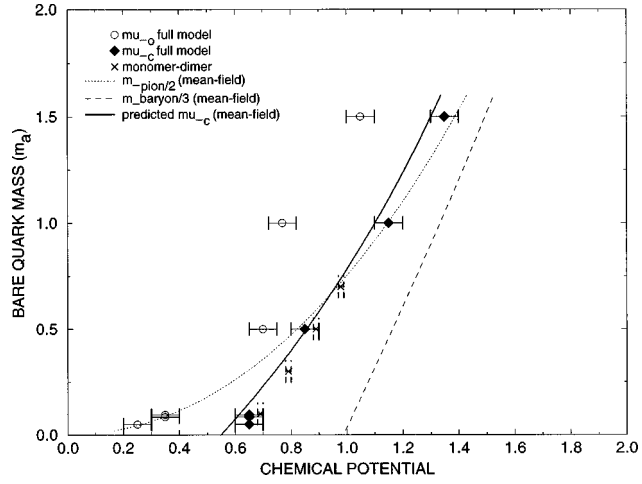

FIG. 6. Summary of the results for the critical point μ_c, and current onset μ_0. μ_c follows the prediction of the mean field analysis of [18] (solid line). The onset is close to half the pion mass at small mass, and below half the pion mass for $m_q>0.5$.

Finally, we have also simulated larger masses. We appreciated the shifting in the central peak, and also its broadening — probably due to the fact that at large quark mass the transition is washed out. Interestingly, the current onset at larger quark mass is, apparently, smaller than half the pion mass — a surprising result since at $m_q=1.5$ in the quenched model the critical region shrinks to zero [6] — certainly this adds to the complication and the confusion associated with μ_0 .

However, even if the interpretation of the critical region at this stage is largely subjective, the estimate of the critical point μ_c seems reasonably sound.

We then conclude our Results section with the summary of Fig. 6.

E. The analysis of the probability distributions

In this section we reexamine the critical region by studying the probability distribution for the particle number.

Write

$$Z=\sum_{n=-3V}^{3V} W_n \tag{22}$$

and normalize such that $Z=1$. W_n is then the probability that a system in a grand canonical ensemble has n particles.

Using the numerical results for the GPF above [see Eq. (8)], the shapes of the probability distributions $W_n=Q_n e^{\mu n_t n}$ for different chemical potentials can be drawn as a function of n, and the critical region can be studied using standard statistical mechanics analysis.

For a transition in a classical ensemble in the infinite volume limit, the distribution of W_n should have a single peak in a pure phase, and a flat distribution at the critical point, where all values of the particle number between the two extrema should be equally likely.

The current $\langle J_0\rangle$ can be written as

$$\langle J_0\rangle=\frac{1}{V}\sum_{n=-3V}^{3V} nW_n\,. \tag{23}$$

We draw in Fig. 7 the probability distribution for small chemical potential. At $\mu=0$ (solid line) the distribution is symmetric around the origin: look at the two satellite peaks of equal height. $\langle J_0\rangle$ equals zero as it should. At $\mu=0.1$ (dashed line) the distribution becomes asymmetric, reflecting the enhancement (suppression) of the forward (backward) propagation: the peak on the left decreases, the one on the right increases. Positive and negative states are still both contributing to the probability distribution. The net $\langle J_0\rangle$ moves immediately off zero, but it is very, very small (look again at picture 2). The distribution broadens on smaller lattices, which accounts for the pattern of finite size effects seen in the same picture.

At $\mu=\mu_0$ the scenario changes completely: a secondary maximum develops at positive n, and the distribution moves to the positive n region. We show this behavior for both $m_q=0.1$ and $m_q=0.08$ in Fig. 8. For $\mu>\mu_0$ the negative

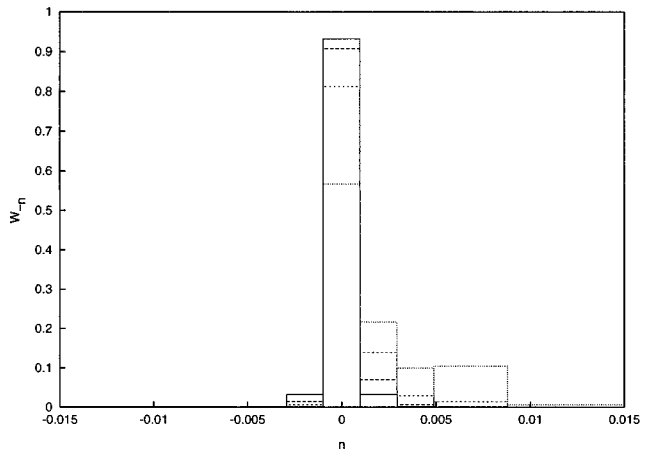

FIG. 7. Probability distributions for a small chemical potential at $m_q=0.1$ on the 8^4 lattice. The solid line is $\mu=0$, the dashed lines, from top to bottom at $n=0$, are for $\mu=0.1$, 0.2, 0.3.

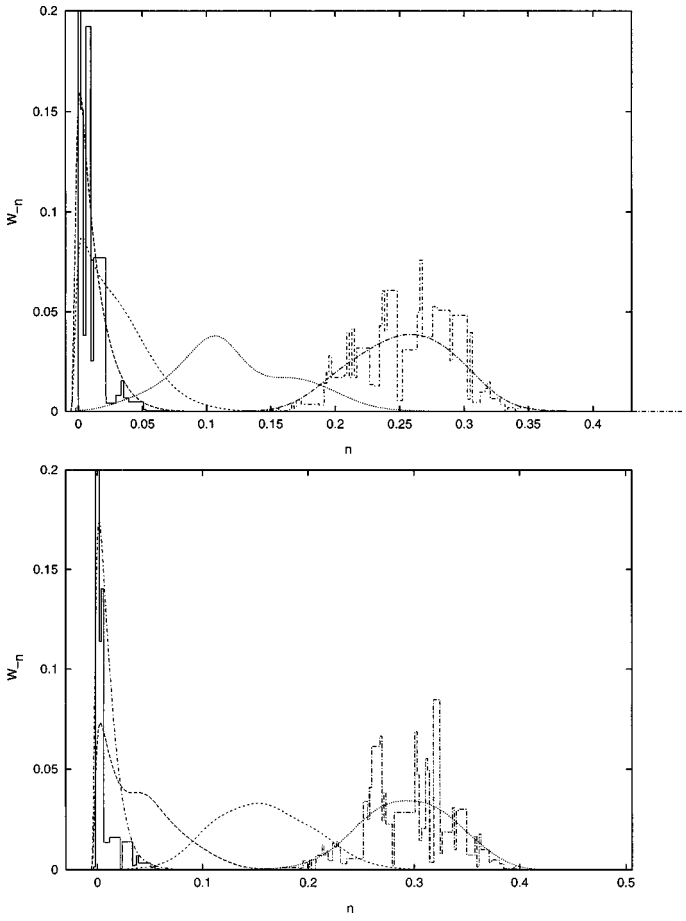

FIG. 8. Probability distributions around the onset μ_0 for $m_q=0.08$ (top) and $m_q=0.1$ (bottom) on an 8^4 lattice. The leftmost histogram (solid) at $m_q=0.08$ is for $\mu=0.28$, the rightmost is for $\mu=0.34$. Bezier interpolations (from Gnuplot) are shown for $\mu=0.28$, 0.30, 0.32, 0.34. At $m_q=0.1$, $\mu=0.32$, 0.34, 0.36, 0.38 from left to right. For both masses at μ_0 the probability distribution moves on the positive n axes.

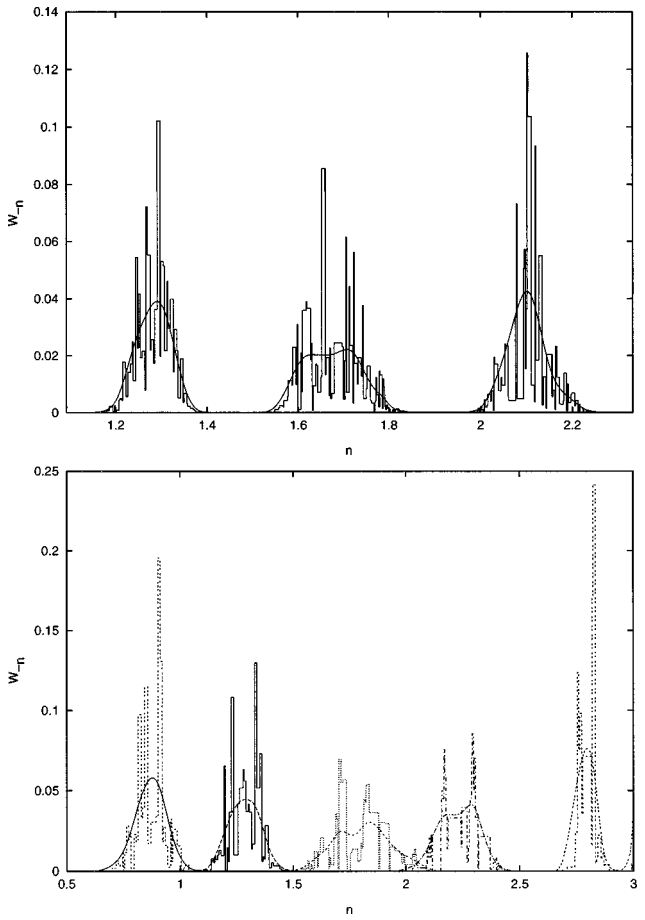

FIG. 9. Probability distributions in the critical region at $m_q=0.1$, on the 8^4 (top) and the 6^4 (bottom). μ is (0.6, 0.683, 0.75), from left to right (top), and (0.5, 0.6, 0.695, 0.75, 1) (bottom).

states do not contribute. This behavior is correlated with the sharp increase of J_0 plotted before and should be related to changes in the theory's spectrum, perhaps reflecting pathologies of the quenched case such as the '' funny pions'' [10] or Stephanov's condensates [29]. The distribution is now roughly symmetric, and its broadening on smaller lattices does not affect its average value $\langle J_0\rangle$. This behavior is compatible with the absence of strong volume effects, Fig. 2.

Next, the critical region: we see the expected broadening of the probability distribution at μ_c (Figs. 9 and 10). Finite size effects become important again for $\mu>\mu_c$. Note, in particular, in Fig. 10, the sensitivity to μ on a very fine scale: the three central plots are for $\mu=0.68$, 0.683, 0.7.

In Fig. 11 we summarize these observations by plotting W_0, the probability that the system has zero particle number, and the integrated probabilities $W^+=\Sigma W_n, n>0$; $W^-=\Sigma W_n, n<0$. The logarithmic scale of the plot makes it easy to see that backward and forward propagations are enhanced and suppressed by the same factor at small μ. Correspondingly, the contribution of $n=0$ must decrease. At $\mu=\mu_0$, $n=0$ equals the overall contribution from >0. For $\mu>\mu_0$ only positive n's contribute to Z.

These results suggest that μ_0 is the threshold for a phase with only positive propagation. Perhaps this observation is a clue to the nature of the phase $\mu>\mu_0$. Recall that mean field analysis predicts the threshold of the mixed phase (broken

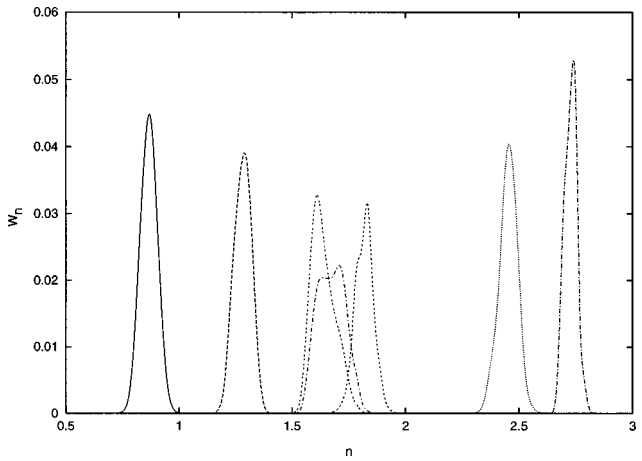

FIG. 10. Probability distributions on the 8^4 lattice, $m_q=0.1$, for μ = (0.5, 0.6, 0.68, 0.683, 0.7, 0.8, 0.9). Only the Bezier interpolations are shown. The complete results for several μ values can be seen in Fig. 9.

phase and/or saturated phase) at $\mu \simeq \mu_0$. Future work should address possible relations between these observations.

We believe that μ_c indicates a physical critical point. All approaches (except the pathological quenched case) predict a transition or, at least, a clear change of behavior of observables here. From the point of view of this section it is relatively easy to understand the robustness of this result: the probabilities plotted here underlie all the observables discussed earlier and the ''flatness'' of the distributions, which locates the critical point, is a qualitative feature which should appear in all the numerical procedures.

IV. OUTLOOK

We have reached a partial understanding of the algorithms and we can point out some successes and failures.

On the positive side, the method gives clear signs of the critical point μ_c which should be the point of chiral symmetry restoration. The method also gives a current onset μ_0 far different from μ_c. This is most likely unphysical: it is not seen in the monomer-dimer results, it is the same as the pathological quenched onset, and it is the threshold of a phase characterized by forward propagation. Unfortunately, since J_0, and other observables such as the energy density, deviate from zero at the unphysical μ_0 point, their values near μ_c cannot be trusted. So, although the present algorithm gives μ_c accurately, it does not make any other phenomenologically reliable predictions.

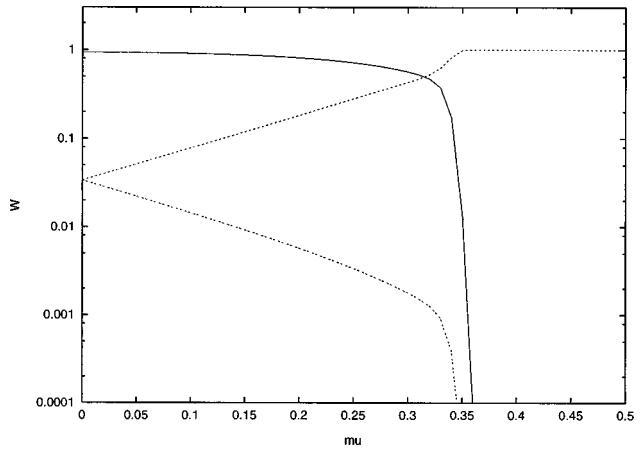

FIG. 11. W_0 (solid), and integrated probabilities W^+ and W^- (dashed) at $m_q=0.1$, on the 8^4 lattice.

We expect that the early onset μ_0 should disappear in a correct calculation. Physical arguments support this view as well as the monomer-dimer and strong coupling expansions discussed here. It might be that a high statistics run of the present algorithm will cancel μ_0. In this case the method would be impractical, but, at least, not conceptually wrong. If this were true, we should develop a strategy to monitor the convergence of the method to the correct statistical ensemble, and to remove unphysical contributions to observables due to partial ''cancellations'' of unwanted onsets.

A very unpleasant possibility, which we cannot exlude *a priori*, is that the results we are observing are indeed the final results at finite chemical potential with the Glasgow method. In this case, monomer-dimer simulations and strong coupling calculations would differ from the Glasgow results. This result would indicate intrinsic difficulties of the finite density lattice gauge theory simulation strategies. Some of these have been discussed in the text.

We might also suspect that the problems stem from having generated configurations at zero chemical potential. This explanation is suggested from the standard problems encountered by reweighting procedures, and from the behavior observed in the Gross-Neveu model [3]. In this case the Glasgow method can be improved if a better starting point were invented. This is a worthwhile direction to pursue.

At the present point, we have to accept that ensemble averaging does not help to suppress the pathologies of isolated configurations. It might well be that a satisfactory simulation of finite density QCD requires an algorithm which produces physical results on each configuration. A promising development of this sort is χQCD [30], where an irrelevant 4F term is added to the standard QCD action used here. χQCD has the advantage that chiral symmetry breaking and the generation of a dynamical quark mass occurs configuration by configuration and the pion and σ excitations are explicitly free of μ dependence. In fact, χQCD simulations do not suffer from the severe μ_0 pathologies seen here [26], but additional work, both theoretical and practical, is needed to see if χQCD really produces only physical results. Research in this topic is in progress.

ACKNOWLEDGMENTS

We wish to acknowledge valuable discussions with N. Bilić, F. Karsch, P. Kornilovitch, G. Parisi, H. Satz, and M. Stephanov. M.P.L. would like to thank the Physics Department of the University of Bielefeld for its hospitality, and the High Energy Group of HLRZ/Jülich, particularly K. Schilling, for support during the initial stages of this project. The calculations were done at HLRZ/KFA Jülich and at King's College, London. This work was partially supported by Nato Grant Nos. CRG950896 and CRG960002 and by PPARC under Grant No. GR/K55554. E.G.K. was supported by EPSRC Grant No. GR/L03026. J.B.K. was partially supported by the National Science Foundation, NSF-PHY92-00148.

[1] E. Laermann, in *Quark Matter 96*, Proceedings of the International Conference on Ultrarelativistic Nucleus-Nucleus Collisions, Heidelberg, Germany, edited by P. Braun-Munziger *et al.* [Nucl. Phys. **A610**, 1c (1996)]; A. Ukawa, in *Lattice '96*, Proceedings of the International Symposium, St. Louis, Missouri, edited by C. Bernard *et al.* [Nucl. Phys. B (Proc. Suppl.) **53**, 106 (1997)].
[2] See, e.g., C. M. Ko, V. Koch, and G. Li, Annu. Rev. Nucl. Part. Sci. (to be published), for a recent review.
[3] I. M. Barbour, S. E. Morrison, E. G. Klepfish, J. B. Kogut, and M.-P. Lombardo, in the Proceedings of the International Conference ''Lattice QCD on Parallel Computers,'' Tsukuba, Japan, 1997, hep-lat/9705042.
[4] J. B. Kogut, H. Matsuoka, M. Stone, H. W. Wyld, S. Shenker, J. Shigemitsu, and D. K. Sinclair, Nucl. Phys. **B225**, 93 (1983).
[5] P. Hasenfratz and F. Karsch, Phys. Lett. **125B**, 308 (1983).
[6] I. Barbour, N. E. Behilil, E. Dagotto, F. Karsch, A. Moreo, A. Stone, and H. W. Wyld, Nucl. Phys. **B275**, 296 (1986).
[7] P. E. Gibbs, Phys. Lett. B **172**, 53 (1986).
[8] C. T. H. Davies and E. G. Klepfish, Phys. Lett. B **256**, 68 (1991).
[9] J. B. Kogut, M.-P. Lombardo, and D. K. Sinclair, Phys. Rev. D **51**, 1282 (1995).
[10] M.-P. Lombardo, J. B. Kogut, and D. K. Sinclair, Phys. Rev. D **54**, 2303 (1996).
[11] I. M. Barbour, C. T. H. Davies, and Z. Sabeur, Phys. Lett. B **215**, 567 (1988).
[12] I. M. Barbour and Z. Sabeur, Nucl. Phys. **B342**, 269 (1990).
[13] I. M. Barbour and A. J. Bell, Nucl. Phys. **B372**, 385 (1992).
[14] A. Hasenfratz and D. Toussaint, Nucl. Phys. **B371**, 539 (1992).
[15] I. M. Barbour, A. J. Bell, and E. G. Klepfish, Nucl. Phys. **B389**, 285 (1993).
[16] I. M. Barbour, S. E. Morrison, and J. B. Kogut, in *Lattice '96* [1], p. 456.
[17] S. E. Morrison, Ph.D. thesis, University of Glasgow, 1997.
[18] P. H. Damgaard, D. Hochberg, and N. Kawamoto, Phys. Lett. **158B**, 239 (1985).
[19] E.-M. Ilgenfritz and J. Kripfganz, Z. Phys. C **29**, 79 (1985).
[20] N. Bilić, K. Demeterfi, and B. Petersson, Nucl. Phys. **B377**, 615 (1992).
[21] F. Karsch and K. H. Mütter, Nucl. Phys. **B313**, 541 (1989).
[22] M.-P. Lombardo, in *RHIC Summer Study '96*, Proceedings of the First Summer Study on the Physics of Ultrarelativistic Nucleus-Nucleus Collisions at RHIC, Upton, New York, edited by D. E. Kahane and Y. Pang (BNL Report No. 5214, Upton, in press), p. 61.
[23] C. N. Yang and T. D. Lee, Phys. Rev. **87**, 404 (1952); T. D. Lee and C. N. Yang, *ibid.* **87**, 410 (1952).
[24] C. Itzykson, R. B. Pearson, and J.-B. Zuber, Nucl. Phys. **B220**, 415 (1983).
[25] S. Hands, S. Kim, and J. B. Kogut, Nucl. Phys. **B442**, 364 (1995).
[26] I. M. Barbour, S. E. Morrison, and J. B. Kogut, ''Lattice Gauge Theory Simulations at Nonzero Chemical Potential in the Chiral Limit,'' hep-lat/9612012.
[27] A. Gocksch, Phys. Rev. D **37**, 1014 (1988).
[28] J. H. Wilkinson, Numer. Math. **1**, 150 (1959).
[29] M. I. Stephanov, Phys. Rev. Lett. **76**, 4472 (1996).
[30] J. B. Kogut and D. K. Sinclair, in *Lattice '96* [1], p. 272.